International Journal of Design & Nature and Ecodynamics
Vol. 21, No. 4, April, 2026, pp. 1029-1036
Journal homepage: http://iieta.org/journals/ijdne

Mechanistic Role of Surface Roughness on CO_2 Corrosion Kinetics and Pitting Susceptibility of AISI 1020 Carbon Steel

Khalid Abdulhussain Mohammed*, Noor Najm, Ahmed M.D. Al Ketife

Oil and Gas Department, College of Engineering, University of Thi-Qar, Nassiriya 64001, Iraq

Corresponding Author Email: dr.khalid@utq.edu.iq

https://doi.org/10.18280/ijdne.210410

Received: 8 February 2026
Revised: 15 April 2026
Accepted: 26 April 2026
Available online: 30 April 2026

Keywords:
CO_2 corrosion, surface profilometry, AISI 1020 carbon steel, pitting susceptibility, anodic activation

ABSTRACT

Surface roughness is often cited as a factor in CO_2 corrosion, but its effect is not consistently accounted for, especially when comparing electrochemical and weight-loss results. In this work, AISI 1020 carbon steel with different surface finishes was tested in CO_2-saturated 3 wt.% NaCl at 25 °C under stagnant conditions. Corrosion behavior was examined using linear polarization resistance (LPR) over the first 180 minutes, polarization measurements, weight loss over 168 hours, and Scanning Electron Microscopy (SEM). As the surface became smoother, the average roughness, Ra, decreased from 2.652 to 0.448 µm. Over the same range, the corrosion rate from weight loss decreased from 0.92 to 0.58 mm/y, while the average LPR corrosion rate decreased from 1.96 to 0.96 mm/y. Polarization results showed that rougher surfaces had more active corrosion potentials, higher corrosion current densities, and lower polarization resistance. SEM observations also revealed more localized attack and deeper pits on the rougher samples, whereas smoother surfaces were affected mainly by more uniform corrosion. These results suggest that surface roughness affects corrosion mainly by increasing anodic activity and promoting localized dissolution within surface features. The differences between electrochemical and gravimetric results are due to changes at the surface during the early stages of exposure, which are captured by LPR but averaged out in weight-loss measurements. The findings are very important in the oil and gas industry via reducing corrosion.

1. INTRODUCTION

Corrosion is a thermodynamically driven degradation process driven by electrochemical interactions between metals and their environment. The corrosion resistance of metallic materials depends on various factors, including electrochemical pathways, the chemical environment, and surface conditions. Beyond material loss, corrosion can compromise the structural integrity and operational safety of critical infrastructure [1].

Every year, corrosion phenomena cost the oil and gas industry tens of billions of dollars in lost income and treatment costs, and the total annual cost of corrosion is expected to exceed $ 2.5 trillion [2-6]. Based on their availability and ability to meet many mechanical, structural, fabrication, and cost requirements, carbon steel alloys are widely used throughout the oil and gas industry, from production and processing to the transportation and distribution of refined products. Unfortunately, internal corrosion of oil and gas pipelines is frequently reported in the petroleum industry, especially in environments containing dissolved carbon dioxide (CO_2) and saline water [7, 8].

Although the mechanisms of CO_2 corrosion have been studied in detail, the influence of initial surface condition, particularly surface roughness, has not been fully quantified. Rougher surfaces increase the effective electrochemical area and alter mass transport near the metal surface. In addition, surface features such as grooves and valleys can form occluded regions where corrosive species accumulate, leading to local chemical changes and promoting pit initiation and growth [9-12]. Inconsistent surface treatments can therefore introduce significant scatter in corrosion data, limiting reproducibility and reducing confidence in translating laboratory results to field conditions.

Inconsistent surface preparation can introduce significant scatter in corrosion data. This makes results less reproducible and more difficult to relate to service conditions. This is important not only for laboratory comparisons but also for assessing material durability, controlling corrosion, and planning long-term maintenance for carbon-steel equipment exposed to CO_2-containing environments. Even though CO_2 corrosion has been widely studied [13-16], the effect of the starting surface condition, especially surface roughness, remains unclear. In CO_2-saturated brine, dissolved CO_2 makes the solution more acidic, which helps the steel dissolve more easily. As this happens, Fe^{2+} is released from the steel into the solution near the surface and can react with carbonate species to form $FeCO_3$ if the local concentration becomes high enough. The amount of protection provided depends on the temperature, pH, and test conditions [8, 17, 18]. At 25 °C and

pH 5, the $FeCO_3$ is not expected to form a compact protective layer, and corrosion remains in the active stage [19]. Under these conditions, a rougher surface can still make a difference. It exposes more real area to the solution and creates grooves and valleys where the solution can stay longer. These sites can then become favorable places for localized attack and pit growth.

However, a clear link between surface roughness and the differences observed between electrochemical and gravimetric corrosion measurements is still lacking [20, 21]. In particular, the extent to which surface conditions contribute to the divergence between short-term linear polarization resistance (LPR) data and long-term weight-loss outcomes has not been systematically examined [21]. This work systematically investigates the influence of surface roughness on the rate and severity of pitting corrosion in AISI 1020 carbon steel under stagnant, CO_2-saturated conditions. By integrating electrochemical, gravimetric, and surface characterization techniques, this study provides mechanistic insight into the role of surface morphology in CO_2 corrosion and underscores the importance of controlled surface preparation for reproducible laboratory testing.

2. EXPERIMENTAL SETUP

2.1 Equipment

The corrosion tests were carried out at atmospheric pressure in a 1 L glass cell. The setup is shown in Figure 1. The solution was 3 wt.% NaCl prepared with deionized water and saturated with CO_2. Before each test, CO_2 was bubbled through the solution for approximately 2 hours at a flow rate of 50 mL/min. Dissolved oxygen was measured before testing by a colorimetric method. The measured value was below the detection limit of the method (DO < 50 ppb). CO_2 bubbling was continued during the test to keep the solution saturated. Gentle stirring was used only during solution preparation. During the corrosion test itself, no mechanical stirring was used, and the specimens were exposed under static conditions.

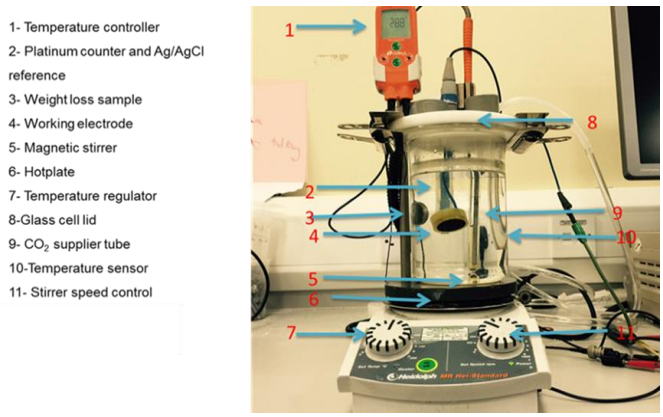

Figure 1. Photograph of the experimental setup for CO_2 corrosion testing in CO_2-saturated 3 wt.% NaCl solution

The solution was heated to 25 °C using a hot plate. The pH was monitored during the test and remained close to 5 ± 0.1 under continuous CO_2 bubbling. No buffer was used. Because the solution was unbuffered, the reported pH reflects the measured bulk condition during exposure rather than active pH control. LPR measurements were carried out over the first 180 minutes to follow the early corrosion behavior. Weight loss measurements and Scanning Electron Microscopy (SEM) observations were performed after 168 hours of exposure.

Each condition was tested at least three times, and the error bars shown correspond to the standard deviation of the corrosion measurements.

2.2 Specimen preparation and surface finishing

All test coupons were machined from AISI 1020 carbon steel and prepared with a cylindrical shape measuring 12 mm in diameter and 10 mm in thickness. AISI 1020 carbon steel was selected due to its widespread use in oil and gas pipeline transmission systems. The chemical composition of the alloy is provided in Table 1 [14]. Cylindrical specimens (12 mm diameter × 10 mm height) were machined and prepared for electrochemical testing. For electrochemical testing, the specimens were mounted so that only the prepared working surface was exposed to the electrolyte. The sides and bottom were coated to define a constant exposed area. Weight-loss coupons were prepared using the same grinding sequence and surface-finishing procedure as for the electrochemical specimens to ensure uniformity and consistency between gravimetric and electrochemical measurements. The schematic of the cylindrical coupons used in this study (12 mm diameter and 10 mm height), with an exposed surface area of 1.13 cm^2 per specimen, is shown in Figure 2.

Before immersion, specimen surfaces were sequentially ground using silicon carbide (SiC) abrasive papers with grit sizes of 100, 300, 600, 800, 1200, and 2400. After grinding, specimens were rinsed with methanol, degreased with acetone, and dried before testing.

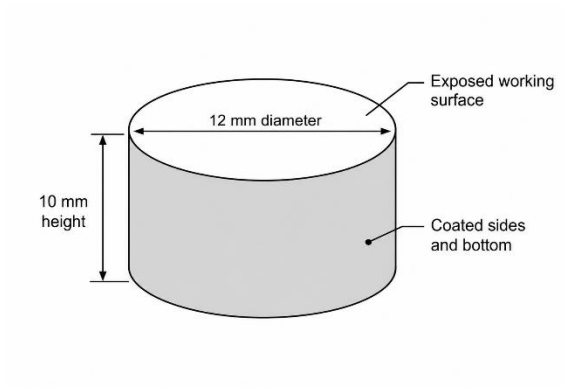

Figure 2. Schematic of the cylindrical specimen used for electrochemical testing, showing the coated sides and bottom, and the exposed top working surface

Table 1. Chemical composition of AISI 1020 steel (wt.%)

Unit	C	Mn	P	S	Fe
wt.%	0.17-0.23	0.3-0.6	≤ 0.04	≤ 0.05	99.08-99.53

2.3 Experimental procedure

Experiments were conducted under stagnant conditions. The experimental conditions and test matrix are summarized in Table 2.

To determine instantaneous corrosion rates, a Gill ACMT 12 multi-channel potentiostat was used in a three-electrode configuration, with an AISI 1020 carbon steel working

electrode (WE), a saturated Ag/AgCl reference electrode (RE), and a platinum counter electrode (CE). The LPR test starts at -15 mV of the open circuit potential (OCP) and ends at 15 mV, with a scan rate of 0.25 mV/s (15 mV/min).

Table 2. Test matrix for CO_2 corrosion testing of AISI 1020 carbon steel in CO_2-saturated 3 wt.% NaCl solution at 25 °C under stagnant conditions

Test Solution	CO_2-Saturated 3 wt.% NaCl Prepared with Deionized Water
Test material	AISI 1020 carbon steel
Temperature	25 °C
Pressure	1 bar
pH	5 ± 0.1
Velocity	Static (no imposed flow)
Test duration	LPR (0–180 min), immersion exposure (weight loss and SEM) (168 hours)
Surface finish	100, 300, 600, 800, 1200, and 2400
Electrochemical techniques	LPR and potentiodynamic polarization
Gravimetric and surface analysis	Weight loss and SEM
LPR perturbation	±15 mV

Prior to each experiment, the exposed surfaces of weight-loss coupons were ground to the target surface finish (100–2400 grit), rinsed with deionized water, cleaned with isopropyl alcohol, dried with compressed air, and coated on the sides and bottom to define the exposed area. Immediately after immersion, the open circuit potential (OCP) was monitored to allow stabilization (typically 1–5 min). LPR measurements were performed during the early stage of exposure to monitor time-dependent corrosion kinetics.

After the full immersion period (168 hours), potentiodynamic polarization measurements were performed. Weight-loss measurements and SEM observations were also conducted after 168 h of exposure.

2.4 Electrochemical measurements

Electrochemical corrosion behavior was evaluated by measuring the corrosion current density (i_{corr}), a key kinetic parameter describing the corrosion rate under the tested conditions. Because corrosion involves simultaneous anodic and cathodic reactions, corrosion occurs at many microscopic sites on the metal surface. i_{corr} cannot be measured directly; it is estimated using electrochemical polarization techniques. Based on Faraday's law, the material dissolution rate is proportional to the measured current density:

$$\textit{Material loss (in moles/cm}^2\textit{/s)} = i/nF \quad (1)$$

where i is the current density (A/cm^2), n is the number of electrons involved in the electrochemical reaction, and F is Faraday's Constant (96,500 C/mol).

The corrosion current density i_{corr} was obtained from LPR measurements using the Stern–Geary relationship [22]:

$$i_{\text{corr}} = \frac{B}{R_p} \quad (2)$$

where R_p is the polarization resistance (Ω.cm^2), and B is the Stern–Geary constant. The parameter B is related to the anodic and cathodic according to:

$$B = \frac{\beta_a \beta_c}{2.303(\beta_a + \beta_c)} \quad (3)$$

where β_a and β_c are the anodic and cathodic Tafel slopes, respectively. The parameter B is related to the anodic and cathodic Tafel slopes according to the Stern–Geary equation. The corrosion potential, E_{corr} was determined from the polarization curve as the potential at which the anodic and cathodic currents are equal, corresponding to zero net current.

In the present study, a fixed value of $B = 0.0151\,V$ was used in the LPR-based corrosion-rate calculations. This value was treated as an assumed Stern–Geary constant rather than a fitted parameter.

The corrosion rate (CR) was calculated using Faraday's law to obtain values in mm/year, accounting for the density of carbon steel ($\rho = 7.86$ g/cm^3) and the equivalent weight of iron.

Electrochemical measurements were performed in the following sequence: (i) stabilization at open circuit potential (OCP), (ii) LPR measurements to obtain R_p and determine corrosion kinetics, and (iii) potentiodynamic polarization to evaluate anodic and cathodic behavior.

2.5 Weight loss measurements

Weight loss measurements and electrochemical experiments were carried out simultaneously. These tests determined the time-averaged corrosion rate by immersing coupons in the same glass cell and under the same conditions.

Gravimetric testing is widely used and reliable because it directly measures cumulative material loss over the exposure period. Before immersion, all coupons were prepared using the same surface-finishing procedure as the electrode specimens. After each experiment, coupons were removed from the electrolyte after 168 hours of immersion. Corrosion products were chemically removed using Clarke's solution (composition shown in Table 3) in line with ASTM G1. The coupons were then rinsed with distilled water, cleaned with isopropyl alcohol, air-dried, and reweighed. If needed, the cleaning and weighing steps were repeated until a stable mass was obtained. The final recorded mass was taken as the value after complete removal of corrosion products.

Coupon masses were measured using a digital balance with a 0.05 mg resolution. The difference between the initial and final masses yielded the average corrosion rate over the entire exposure period. Gravimetric corrosion rates represent the mean value of repeated measurements for each surface finish.

Table 3. Composition of Clarke's solution

Component	Amount
Hydrochloric acid (HCl, sp. gr 1.19)	1 liter
Antimony trioxide (Sb_2O_3)	20 g
Stannous chloride ($SnCl_2$)	50 g

After cleaning, the coupons were rinsed with distilled water, cleaned with isopropyl alcohol, air-dried, and then reweighed. The mass loss before and after exposure was calculated and converted to the corrosion rate (CR) using:

$$CR = \frac{mb - ma}{A\rho_{F_e}{}^{t}} 8.7 \times 10^4 \quad (4)$$

where, CR is corrosion rate (mm/y); mb and ma are the masses of specimens before immersing in the test solution and after Clarke's solution cleaning, respectively (kg); A is the surface area of the specimen (m^2); ρ_{Fe} is the iron density (kg/m^3), and t is the exposure time(s).

3. RESULTS AND DISCUSSION

3.1 Surface roughness measurement (profilometry)

Surface roughness was measured using a Mitutoyo SJ-210 contact profilometer (Table 4). Roughness profiles used a cut-off length (λc) of 0.8 mm and an evaluation length of 4.0 mm. The instrument had a stylus with a 2 µm tip radius, and measurements were made at a scan speed of 0.5 mm/s. Six measurements (n = 6) were taken in random locations for each surface finish. summarizes the mean values of average roughness (Ra) and maximum peak-to-valley height (Rz).

The result showed that as the abrasive grit number increased, the surfaces became smoother. This is shown by the decrease in average roughness (Ra), which dropped from 2.652 µm for the 100-grit finish to 0.448 µm for the 2400-grit finish. A similar trend was observed for Rz, which decreased from 36.22 µm to 4.024 µm, indicating that the height of surface asperities was reduced with finer polishing.

The spread in roughness values decreased at higher grit sizes, as indicated by the lower standard deviation, suggesting that the surfaces were more consistent after finer preparation. These measured roughness differences provide the basis for analyzing the electrochemical response and the corrosion rates obtained from weight-loss measurements.

Table 4. Measured surface roughness parameters (Ra and Rz) of AISI 1020 carbon steel for different SiC grit surface finishes

	Surface Finish (grit)					
	100	300	600	800	1200	2400
Average Ra (µm)	2.652 ± 1.24	2.284 ± 1.18	1.442 ± 0.81	1.024 ± 0.55	0.825 ± 0.38	0.448 ± 0.32
Average Rz (µm)	36.22	25.12	18.82	11.92	6.652	4.024
SD of Ra	1.244	1.181	0.812	0.548	0.388	0.232

Reported as mean ± SD (n = 6)

3.2 Time-resolved corrosion kinetics from linear polarization resistance

The influence of surface condition on corrosion kinetics in CO_2-saturated brine is shown in Figure 3, where corrosion rates were monitored over 3 hours using LPR. During early exposure, the results demonstrate that the corrosion rate changes over time, reflecting transient interfacial modifications such as variations in the effective electrochemically active area, the development of corrosion products, and partial surface activation or coverage. Overall, rougher finishes tend to have higher corrosion activity, with the 100-grit surface displaying the highest LPR-derived corrosion rate and the 2400-grit surface showing the lowest throughout the monitoring period. To allow for quantitative comparison across different surface finishes, LPR corrosion rates were reported as the average over 0–180 minutes, denoted CR (LPR,avg). Time-resolved electrochemical measurements reflect the instantaneous corrosion behavior and can therefore show short-term fluctuations that are not captured by time-averaged gravimetric methods. When localized corrosion contributes significantly to the measured current, corrosion trends derived from short-term LPR measurements may differ from those based on long-term weight-loss measurements.

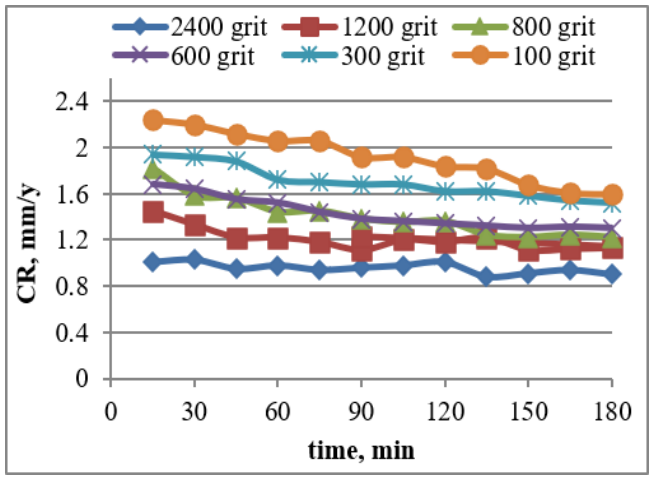

Figure 3. Average corrosion rate of AISI 1020 carbon steel in CO_2-saturated 3 wt.% NaCl solution at 25 °C at several surface roughness

3.3 Comparison of corrosion rates obtained from different methods

Figure 4 shows the corrosion rates measured using both weight loss and electrochemical methods for the different surface finishes. The weight-loss results decrease as the surface becomes smoother, indicating that rougher surfaces lose more material over time. This is due to their larger effective surface area and tendency to promote localized attack, as seen in the SEM results. In comparison, LPR-derived corrosion rates exhibit greater time dependence and variability due to their sensitivity to transient surface conditions during early exposure.

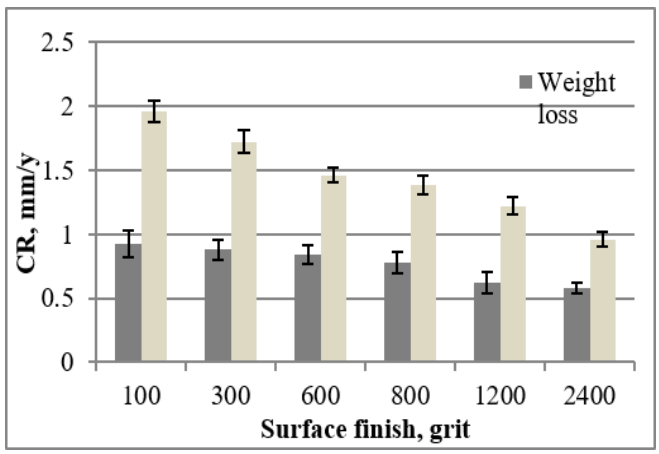

Figure 4. Different surface finishes in CO_2-saturated 3 wt.% NaCl solution at 25 °C under stagnant conditions

Using both weight-loss and electrochemical data provides a clearer picture of what is really happening, since one shows how the surface behaves at a given time and the other shows how much material is actually lost.

Table 5 shows the corrosion rates from weight loss and LPR for AISI 1020 steel in CO_2-saturated 3 wt.% NaCl at 25 °C. Both sets of results follow the same trend. As the surface becomes rougher, the corrosion rate increases. The 100-grit samples show the highest values, while the 2400-grit samples show the lowest, which means the starting surface condition has a clear effect under these conditions.

The difference between the two methods is quite large, ranging from 66% to 114%, with LPR consistently giving higher values. This is not surprising. LPR reflects what is happening at the surface at that moment and is affected by changes early in the test, whereas weight loss reflects the total loss after the full exposure time. Looking at both together makes it easier to understand the corrosion behavior in these CO_2 conditions.

The results suggest that surface roughness contributes directly to the differences observed between electrochemical and gravimetric corrosion rates, particularly through its influence on early-stage surface activity captured by LPR.

From the polarization data in Table 6, the trend is straightforward. As the surface gets rougher, E_{corr} shifts in the active direction, i_{corr} increases, and Rp drops. This means the rougher surfaces are more reactive. The SEM results point in the same direction, with more localized damage on these samples. Taken together, the results show that surface roughness affects both the corrosion rate and the rate of corrosion development. It also affects how the different methods compare. For this reason, the surface finish needs to be kept consistent if the results are to be compared or used in practice.

To further demonstrate the effect of surface roughness on the measured corrosion response, correlation plots were generated between the roughness parameters and the corrosion rates obtained from weight-loss and LPR measurements, as well as the relative differences between the two methods (Figure 5). In all cases, the plots showed that smoother surfaces were associated with lower corrosion rates, while rougher surfaces yielded higher corrosion rates and larger differences between short-term electrochemical and long-term gravimetric measurements.

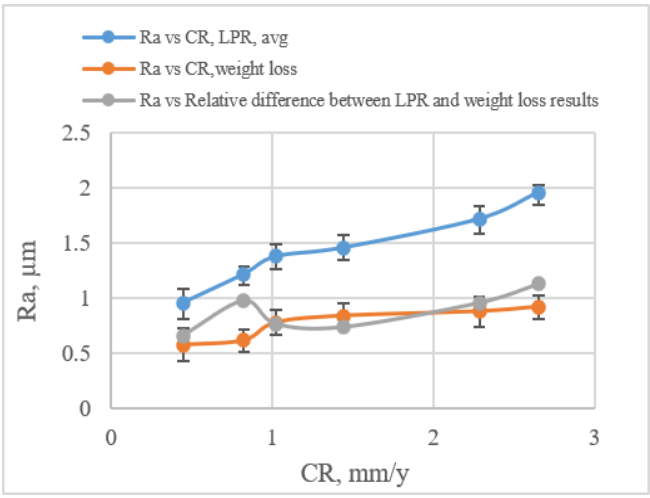

Figure 5. Correlation between surface roughness and corrosion metrics (mean ± SD, n = 6) of AISI 1020 carbon steel in CO_2-saturated 3 wt.% NaCl at 25 °C

Table 5. Comparison of corrosion rates obtained from gravimetric weight loss and time-averaged LPR measurements for AISI 1020 carbon steel in CO_2-saturated 3 wt.% NaCl solution at 25 °C

Surface Finish (SiC grit)	Ra (µm)	CR (Weight Loss) (mm/y)	CR (LPR, Avg 0–180 min) (mm/y)	Relative Difference (%)
100	2.652	0.92 ± 0.06	1.96 ± 0.11	113.8
300	2.284	0.88 ± 0.09	1.72 ± 0.13	96.0
600	1.442	0.84 ± 0.09	1.46 ± 0.11	74.1
800	1.024	0.78 ± 0.08	1.38 ± 0.11	77.5
1200	0.825	0.62 ± 0.06	1.22 ± 0.08	98.0
2400	0.448	0.58 ± 0.06	0.96 ± 0.11	66.3

Reported as mean ± SD (n = 3).
The relative difference between the corrosion rates obtained from LPR and weight-loss measurements was calculated using:
$$Relative\ difference\ (\%) = \frac{CR_{LPR,avg} - CR_{weight\ loss}}{CR_{weight\ loss}} \times 100.$$

3.4 Electrochemical polarization behavior and anodic activation

Potentiodynamic polarization curves for AISI 1020 steel with different surface finishes are shown in Figure 6. The cathodic branches show only minor variation among the tested surfaces, whereas the anodic current density increases more noticeably as surface roughness increases. This suggests that the effect of surface roughness is expressed more strongly on the anodic branch than on the cathodic branch.

It is clear from Figure 6 that the corrosion potential (E_{corr}) shifts towards more positive values with decreasing surface roughness, accompanied by a decrease in the corrosion current density (i_{corr}) and an increase in the polarization resistance (R_p) (Table 6), which is consistent with the reduced corrosion activity of smoother surfaces. Notably, the roughest surface showed a sharp increase in anodic current density directly above E_{corr}, indicating increased melting and a greater tendency towards localized breakdown.

Rougher surfaces have more pronounced asperities and grooves, which can create small occluded areas. These regions tend to trap chloride ions, allowing local acidification to develop, which makes it easier for pits to form and grow under CO_2-saturated conditions. The SEM observations agree with this, showing more localized damage on the rougher samples.

Under the present test conditions of 25 °C and pH around 5, $FeCO_3$ is not expected to form a dense protective film. Any corrosion product that forms is likely to be limited or only weakly protective, so the corrosion process is expected to remain mainly in an active dissolution state. Surface roughness may still affect the local formation and retention of early corrosion products by increasing the real surface area and creating grooves and valleys where solution and dissolved species can accumulate. These features may also make a localized attack more likely.

Overall, the electrochemical results, weight loss data, and SEM analysis indicate that surface roughness plays an active role in corrosion, affecting both the rate and the type of attack. This shows that surface roughness is not just a geometric feature, but an important factor in corrosion behavior. For this

reason, surface preparation needs to be carefully controlled to ensure consistent laboratory results and better comparison with real pipeline conditions.

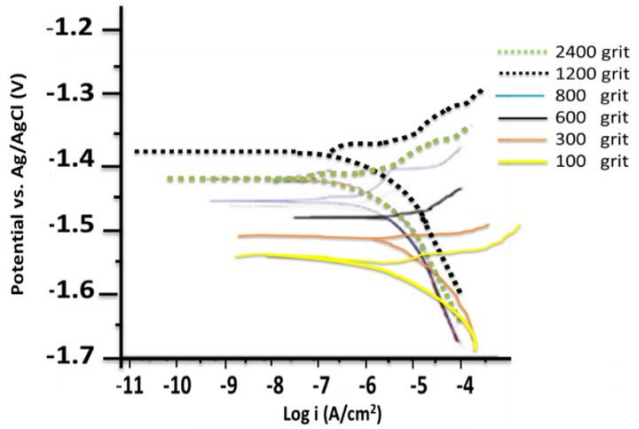

Figure 6. Potentiodynamic polarization curves of AISI 1020 carbon steel with different surface finishes measured in CO_2-saturated 3 wt.% NaCl solution at 25 °C under static conditions

Table 6. Potentiodynamic polarization parameters (E_{corr} and i_{corr}) and calculated polarization resistance (R_p) for AISI 1020 carbon steel with different surface finishes in CO_2-saturated 3 wt.% NaCl at 25 °C

Surface Finish (SiC grit)	Ra (µm)	E_{corr} (V vs Ag/AgCl)	i_{corr} (mA/cm)	R_p (Ω·cm²)
100	2.652	-1.55	0.24	62.9
300	2.284	-1.48	0.18	83.7
600	1.442	-1.45	0.15	100.5
800	1.024	-1.42	0.12	125.6
1200	0.825	-1.38	0.09	167.5
2400	0.448	-1.32	0.06	176.5

3.5 Surface morphology before and after exposure

Representative SEM images of the specimens before immersion are shown in Figure 7. The initial surface morphology is strongly influenced by abrasive grit size, with coarse finishes exhibiting deeper grooves and more pronounced asperities than finer finishes.

SEM micrographs after immersion in CO_2-saturated 3 wt.% NaCl solution for 168 hours under open circuit conditions is presented in Figure 8. The post-exposure surfaces clearly reveal pronounced differences in corrosion morphology as a function of initial surface roughness. Rough finishes exhibit more extensive localized attack and greater pit development, while the smoothest finish shows predominantly uniform corrosion with minimal evidence of pitting. Intermediate finishes exhibit mixed behavior, indicating a transition from localized to more uniform dissolution. SEM Imaging of AISI 1020 carbon steel alloy surface (500× Magnification) before immersion, showing surface morphology produced by different SiC grit finishes.

These SEM images indicate that rough surfaces are more susceptible to pit formation. Grooves and valleys produced by grinding serve as sheltered regions where solution can accumulate. In these areas, chloride ions can accumulate, altering local conditions and facilitating pit initiation and growth under CO_2 environments.

Results demonstrate that surface roughness clearly affects both the rate of corrosion and its appearance. Rougher finishes have more of these surface features, so localized attack is more common, and corrosion rates are higher in both weight loss and LPR results. The polarization data also show higher anodic currents and more active E_{corr} values as roughness increases, while the cathodic side is less affected.

The difference between the electrochemical and weight-loss results stems from how the methods work. LPR reflects what is happening at the surface at a given time, especially early on, while weight loss shows the total damage after the full exposure. For this reason, surface preparation needs to be kept consistent so that results can be compared and related to real pipeline conditions more reliably.

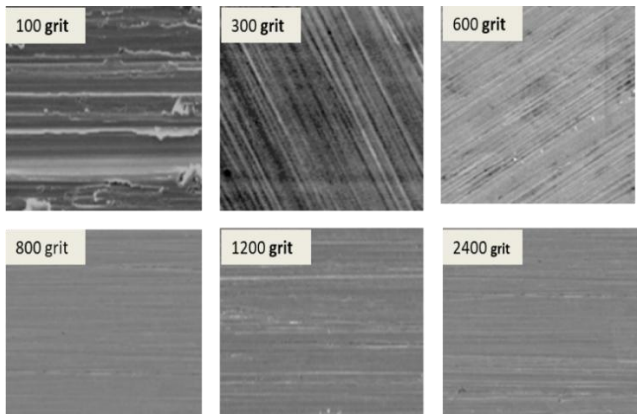

Figure 7. Scanning Electron Microscopy (SEM) images of AISI 1020 carbon steel alloy surface (500× Magnification) before immersion, showing surface morphology produced by different SiC grit finishes

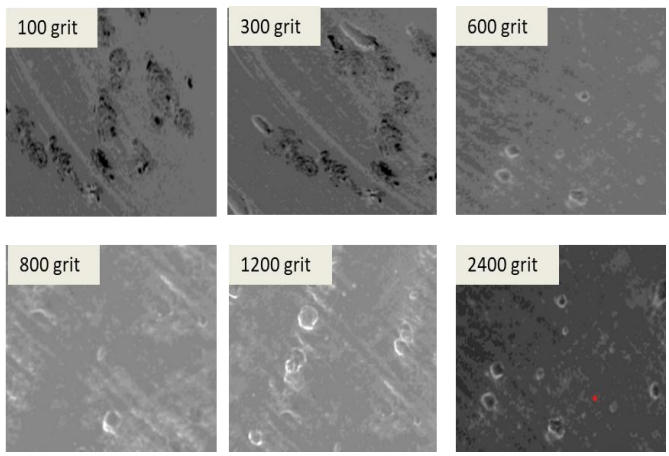

Figure 8. Scanning Electron Microscopy (SEM) micrographs of AISI 1020 carbon steel alloy for different surface roughness after 168 hours immersion in CO_2-saturated 3 wt.% NaCl solution at 25 °C under static conditions for different surface finishes (100–2400 grit)

4. CONCLUSIONS

The results show that surface roughness has a direct and measurable effect on the corrosion behavior of AISI 1020 carbon steel in CO_2-saturated 3 wt.% NaCl at 25 °C. As the surface became smoother, the average roughness (Ra) decreased from 2.652 to 0.448 µm, while the corrosion rate

from weight loss dropped from 0.92 to 0.58 mm/y. Under the same conditions, the average LPR corrosion rate decreased from 1.96 to 0.96 mm/y.

The electrochemical data indicate that this effect is mainly controlled by changes on the anodic side. As roughness increases, E_{corr} shifts in the active direction, i_{corr} increases, and Rp decreases. This points to a more reactive surface, which is supported by SEM observations showing deeper and more frequent pits on rough finishes.

A clear difference was observed between LPR and weight-loss measurements. The relative difference between the two methods ranged from 66.3% to 113.8%, indicating that surface condition affects how corrosion is captured and interpreted.

Overall, the results demonstrate that surface roughness is not just a preparation detail, but a factor that controls both corrosion rate and corrosion form. It also influences how different measurement methods compare. For this reason, surface preparation needs to be controlled and reported carefully in corrosion studies, especially when results are compared or used to represent field conditions.

ACKNOWLEDGMENTS

Scientific support from the University of Thi-Qar for this research is highly appreciated.

REFERENCES

[1] Hansson, C.M. (2011). The impact of corrosion on society. Metallurgical and Materials Transactions A, 42: 2952-2962. https://doi.org/10.1007/s11661-011-0703-2

[2] Iannuzzi, M., Frankel, G.S. (2022). The carbon footprint of steel corrosion. npj Materials Degradation, 6(1): 101. https://doi.org/10.1038/s41529-022-00318-1

[3] Kania, H. (2023). Corrosion and anticorrosion of alloys/metals: The important global issue. Coatings, 13(2): 216. https://doi.org/10.3390/coatings13020216

[4] Mohammed, K.A. (2018). Experimental and theoretical investigation of top of the line corrosion in CO2 gas and oil environments University of Leeds. https://etheses.whiterose.ac.uk/20479/1/Experimental%20and%20theoretical%20TLC%20investigation.pdf.

[5] NACE. (2014). NACE international commences global study on corrosion costs and preventive strategies. Materials Performance, 53(1): 84. https://doi.org/10.5006/MP2014_53_1-84

[6] Sun, P., Wang, Z., Lu, Y., Shen, S., Yang, R., Xue, A., Wang, Q. (2020). Analysis of the corrosion failure of a semiconductor polycrystalline distillation column. Process Safety and Environmental Protection, 135: 244-256. https://doi.org/10.1016/j.psep.2020.01.007

[7] Fezea, M., Gathwan, M.A., Abeed, B.S., Ahmed, L.Q. (2026). Indoor air quality in charcoal-grilling restaurants of Baghdad: Short-term monitoring of PM2.5, PM10, CO2, and CO. International Journal of Design & Nature and Ecodynamics, 21(2): 495-502. https://doi.org/10.18280/ijdne.210217

[8] Mohammed, K.K.A. (2025). The synergistic influence of chloride ion concentration and environmental temperature on the corrosion mechanisms of X65 carbon steel in CO2-saturated oilfield environments. Zastita Materijala. https://doi.org/10.62638/ZasMat1528

[9] Bai, H., Cui, X., Wang, R., Lv, N., Yang, X., Li, R., Ma, Y. (2023). Effect of surface roughness on static corrosion behavior of J55 carbon steel in CO2-containing geothermal water at 65 ℃. Coatings, 13(5): 821. https://doi.org/10.3390/coatings13050821

[10] Gupta, K.K., Pedroni, S., Mercier, A., Haratian, S., Mishin, O.V., Ambat, R. (2025). Effect of surface finish on CO2 corrosion of low-alloy steel in simulated sea water and well environments. Metals, 15(3): 302. https://doi.org/10.3390/met15030302

[11] Kannan, M.B. (2010). Influence of microstructure on the in-vitro degradation behaviour of magnesium alloys. Materials Letters, 64(6): 739-742. https://doi.org/10.1016/j.matlet.2010.01.022

[12] Song, G., Atrens, A., Dargusch, M. (1998). Influence of microstructure on the corrosion of diecast AZ91D. Corrosion Science, 41(2): 249-273. https://doi.org/10.1016/S0010-938X(98)00121-8

[13] Hong, T., Nagumo, M. (1997). Effect of surface roughness on early stages of pitting corrosion of type 301 stainless steel. Corrosion Science, 39(9): 1665-1672. https://doi.org/10.1016/S0010-938X(97)00072-3

[14] Mohammed, K.A., Okab, A.K., Hamad, H.S., Hashim, M., Abdulhussain, R.K. (2021). Drilling and casing pipes corrosion investi-gation in water based drilling mud of Iraqi oil fields environment. Journal of Mechanical Engineering Research and Developments, 44(8): 232-240.

[15] Sasaki, K., Burstein, G. (1996). The generation of surface roughness during slurry erosion-corrosion and its effect on the pitting potential. Corrosion Science, 38(12): 2111-2120. https://doi.org/10.1016/S0010-938X(96)00066-2

[16] Shahryari, A., Kamal, W., Omanovic, S. (2008). The effect of surface roughness on the efficiency of the cyclic potentiodynamic passivation (CPP) method in the improvement of general and pitting corrosion resistance of 316LVM stainless steel. Materials Letters, 62(23): 3906-3909. https://doi.org/10.1016/j.matlet.2008.05.032

[17] Zuo, Y., Wang, H., Xiong, J. (2002). The aspect ratio of surface grooves and metastable pitting of stainless steel. Corrosion Science, 44(1): 25-35. https://doi.org/10.1016/S0010-938X(01)00039-7

[18] Moradighadi, N., Wang, H., Wang, L., Seyeux, A., Pailleret, A., Marcus, P., Nesic, S. (2024). Investigation of iron dissolution mechanism in acidic solutions with and without dissolved CO2—Part I: Electrochemical impedance spectroscopy measurements. Corrosion, 80(7): 705-723. https://doi.org/10.5006/4511

[19] Fonseca, D., Tagliari, M.R., Guaglianoni, W.C., Tamborim, S.M., Borges, M.F. (2024). Carbon dioxide corrosion mechanisms: historical development and key parameters of CO2-H2O systems. International Journal of Corrosion, 2024(1): 5537767. https://doi.org/10.1155/2024/5537767

[20] Igwilo, C.K., Nduji, O.D., Uwaezuoke, N., Dike, C.F. (2025). Performance evaluation of Mucuna solanie and periwinkle shell inhibitors as anti-coating agents for corrosion inhibition. Improved Oil and Gas Recovery, 9. https://doi.org/10.14800/IOGR.1359

[21] Uwaezuoke, N., Onya, O.E., Nnaji, O.C., Dike, C.F., Onwukwe, I.S. (2024). Performance evaluation of palm kernel shell as pitting corrosion Inhibitor. Improved Oil and Gas Recovery, 8. https://doi.org/10.14800/IOGR.1336

[22] Stern, M., Geary, A.L. (1957). Electrochemical polarization: I. A theoretical analysis of the shape of polarization curves. Journal of The Electrochemical Society, 104: 56-63. https://doi.org/10.1149/1.2428496

NOMENCLATURE

Abbreviations

AISI	American Iron and Steel Institute
LPR	linear polarization resistance
SEM	scanning electron microscopy
OCP	the open circuit potential
RE	reference electrode
CE	platinum counter electrode
CR	the corrosion rate, mm/y
OCP	open circuit potential
ASTM	American Society for Testing and Materials

Symbols

wt.%	weight percentage
SiC	silicon carbide
C	carbon concentration, wt.%
Mn	manganese concentration, wt.%
P	phosphorus concentration, wt.%
Fe	iron concentration, wt.%
$NaHCO_3$	sodium bicarbonate species
E_{corr}	the free corrosion potential
i_{corr}	the corrosion current density
R_p	polarization resistance, $\Omega.cm^2$
B	the Stern–Geary constant
β_a and β_c	cathodic Tafel slopes
HCl	hydrochloric acid
Sb_2O_3	antimony trioxide
$SnCl_2$	stannous chloride
A	the surface area of the specimen, m^2
ρ_{Fe}	iron density, kg/m^3
t	the exposure time, s
Ra	average roughness
Rz	maximum peak-to-valley height